

# Time Resolved Experiments in the Picosecond to Microsecond Range using Pulsed Synchrotron Radiation

F. Schotte<sup>\*</sup>, S. Techert<sup>\*</sup>, P. Anfinrud<sup>#</sup>, V. Srajer<sup>&</sup>, K. Moffat<sup>&</sup> and M. Wulff<sup>\*</sup>

<sup>\*</sup>European Synchrotron Radiation Facility, BP 220, Grenoble 38043

<sup>#</sup>Laboratory of Chemical Physics, NIDDK, National Institutes of Health, Bethesda, MD 20892-0520

<sup>&</sup>University of Chicago, CARS, 5640 South Ellis Avenue, Chicago, IL 60637

**Abstract:** We present a review of the beamline components needed for 50 picosecond experiments on a third generation synchrotron. The performance of future in-vacuum undulators is compared with state of the art undulators at the ESRF. It is shown that in-vacuum undulators will increase the available flux by 5-10 and greatly increase the amount of usable beamtime for pump and probe experiments. The x-ray optics in the ID09 beamline is described together with its chopper and femtosecond laser. Finally we discuss the feasibility of pump & probe experiments to 200 fs resolution using the hard x-ray pulse from a free electron laser.

## 1. Introduction

This article describes initial time-resolved structural studies of chemical and biochemical systems using hard x-ray pulses from a third generation synchrotron. With the advent of highly-intense undulator beams from synchrotrons such as the European Synchrotron Facility (ESRF) in France, the Advanced Photon Source (APS) in the USA and SPring8 in Japan, the scientific community has a new tool for the investigation of the structural basis of reaction mechanisms with a time resolution down to 50 picosecond, the duration of a single x-ray pulse. We show how the pulsed structure of synchrotron radiation can be used to probe very short-lived intermediate structures in a reaction pathway in systems ranging from solid state crystals (small molecules and macromolecules), liquids (molecules in solution and elemental liquids) and gas phase reactions. A short laser pulse is used in all cases to initiate the reactions: the energy of the absorbed photon is sufficient to elevate the energy of the reacting molecules above an initiation barrier. The laser pulse also synchronises the initiation and provides a well defined time zero of reactants and products. While the “before” and “after” structures are known for most reactions, the pathways by which they interconvert are largely unknown and, till now, largely unexplored. The ability to watch the structural evolution of macromolecules by a sequence of static data sets each still representing a snapshot at a given time in the reaction scheme, was initially developed at the ESRF[1,2] and is now actively pursued at APS and SPring8. The successful conduct of such fast, time-resolved experiments has required several critical technical advances. The sample must be illuminated by an intense, hard x-ray beam derived from one of more insertion devices and delivered to the sample via suitable x-ray optical elements. The time-structure and duration of the x-ray pulse must be controlled both by the mode of operation of the storage ring and by a fast shutter train; the sample must be stimulated, uniformly and rapidly, by an intense laser pulse, to achieve reaction initiation; the time delay between the arrival of the laser pulse – the pump – and the x-ray pulse – the probe – must be suitably adjustable; and the x-rays that have interacted with the sample must be collected on a sensitive low-noise detector. In addition, the sample itself must be robust, to permit the accumulation of the numerous individual measurements that comprise a complete data set. That is, the sample must withstand illumination by numerous x-ray and laser pulses without exhibiting significant radiation damage.

We consider these technical advances, and illustrate their application to several classes of experiments, in time-resolved macromolecular crystallography and in diffuse scattering from liquids. Our discussion is limited to the ESRF and initial experiments conducted there, but we emphasise that similar experiments may be conducted at other sources, including the newest high brilliance, high-energy sources such as the Swiss Light Source.

## 2. The Pulse Structure of Synchrotron Radiation

The ESRF synchrotron consists of three synchronised accelerators, a 200 m linear accelerator (linac) operated at 200 MeV, a 300 m booster synchrotron in which the energy is raised to 6 GeV and a 844.1 m storage ring. The pulsed structure of the x-rays emitted by the particles in the storage ring is derived ultimately from the 992 potential bunch positions (buckets) in the storage ring, which may be filled with electrons in a variety of ways as illustrated in fig. 1. These patterns differ in their total current, electron bunch structures (and hence x-ray pulse structure) and lifetime. Different fill patterns optimise different classes of experiments, and some fill patterns may be completely unsuitable for certain classes of experiments. For example, many experiments require high current and long lifetime and are incompatible with single bunch mode, conversely, the most demanding time-resolved experiments require single bunch mode and must then tolerate lower current and reduced lifetime. The storage ring master clock frequency is a harmonic of the orbit frequency. At the ESRF it runs at 352.20 MHz, the 992<sup>nd</sup> harmonic of the orbit frequency (355.04 kHz). The filling of the storage ring is obtained in the following way. The linac injects a 1.0  $\mu$ s pulse of 200 MeV electrons into the booster, initially configured for a closed orbit at 200 MeV. The RF field, which runs at the same frequency as in the storage ring, is then switched on and the energy is ramped up to 6 GeV in synchrony with the magnetic field in the bending magnets. It takes 50 ms to reach 6 GeV and the injection into the storage ring is done at 1 Hz. The oscillatory RF field compresses the electron density in the booster into 352 buckets at the phase stable point: the first electrons in the 30 mm long bunch are sent into the RF field while the accelerating field is increasing. Those electrons in the latter part of the bunch experience therefore a slightly stronger field which compensates for their delay. The booster is then filled again and the bunch pattern accumulated in the storage ring. The acceleration, injection, accumulation and finally the bunch cleaning take typically 2-3 min for multi-bunch structures. In the case of the 1-bunch and 16-bunch mode, the electron gun produces a 1.8 ns pulse, which is accelerated in the booster and then accumulated in the storage ring. The injection time is much longer here because of the low number of electrons in a 1 ns linac shot and the time it takes to accumulate a 15 mA current in one bunch.

The lifetime of the beam depends strongly on the vacuum, the energy acceptance of the machine tune and the charge in the bunch. In the 2/3 filling the lifetime is determined by the vacuum mainly (Bremsstrahlung [3] and Rutherford scattering). It is presently about 55 h starting from a 200 mA fill. The lifetime of the single bunch mode is dominated by Touschek scattering, i.e. outward scattering from the Coulomb repulsion within the bunch. The lifetime is typically 6 h measured at 16 mA. The reduced lifetime may be of less experimental consequence if more frequent (re-) filling of the storage ring is possible and indeed the possibility of continuous injection of the storage ring is being investigated in most facilities. Note also that the fill patterns differ markedly in the length of the "dark" periods that flank the electron bunch (or bunches) from which the desired x-ray pulse (or pulse train) is to be extrapolated. The duration of these dark periods determines a key parameter of the x-ray shutter train, described below.

The most frequently used operation mode at the ESRF is a 660 bunch structure in 2/3 of the ring. The APS has chosen a 75 bunch mode in which 25 triplets, in which each bunch is spaced by 2.84 ns, are evenly

distributed around the ring. Finally SPring8 uses 2016 bunches in 24/29 of the ring. The most frequently used bunch structures are shown in fig. 1 and the pulse length is shown in fig. 2.

**TABLE 1.** Source parameters of the three large third generation synchrotrons. The bunch length is quoted as rms(fwhm=2.355  $\sigma$ ).

Source	ESRF	APS	SPring8
Energy (GeV)	6	7	8
Circumference (m)	844.1	1104.0	1436.0
Revolution time ( $\mu$ sec)	2.816	3.683	4.790
Harmonic number(RF)	992	1296	2436
Radio frequency(MHz)	352.2	351.9	508.6
Min-bunch spacing(ns)	2.839	2.842	1.966
Multi-bunch current(mA)	205	100	100
Multi-bunch lifetime(hours)	55	40	110
Single-bunch current(mA)	16	5	15
Single-bunch lifetime(hours)	6.5 (8 mA), 6 (15 mA) ?		11(1mA), 2(15mA)
Zero current bunch length $\sigma_L$ (ps)	25.5	44.6	17.0
No of insertion device beamlines	29	35	38
Length of straight section(m)	6.1	6.7	6.65(30)
Undulator length(m)	3 * 1.6	2* 2.4	1* 4.5(30)
Minimum undulator gap(mm)	6.0	10.5	8.0

**TABLE 2.** Electron source parameters of third generation synchrotrons. Distributions are quoted as rms.

Source	ESRF(low- $\beta$ )	ESRF(high- $\beta$ )	APS	SPring8(high- $\beta_x$ , low- $\beta_z$ )
$\epsilon_x$ (nm rad)	3.8	3.8	8.0	6.0
$\epsilon_z$ (nm rad)	0.011	0.011	0.08	0.006, 0.0024(bare lattice)
coupling ( $\epsilon_z / \epsilon_x$ )	0.003	0.003	0.01	0.001, 0.0004(bare lattice)
$\sigma_x$ ( $\mu$ m)	56.5	391.7	325.0	366.4
$\sigma_z$ ( $\mu$ m)	10.2	9.8	86.0	4.7
$\sigma_x'$ ( $\mu$ rad)	87.6	10.4	23.0	14.9
$\sigma_z'$ ( $\mu$ rad)	3.8	3.9	9.0	1.17

### 3. In-vacuum undulators for time-resolved experiments

The third generation synchrotrons were built to provide intense, collimated and stable undulator beams at wavelengths around 1Å and to provide optics to focus the beam and manipulate the energy distribution and pulse structure at the sample. The characteristics of the insertion device, the bandwidth, the tunability, the flux and the collimation can, within certain limits, be optimised for specific experiments. X-ray spectroscopy goes primarily for tuneability, small angle scattering gives priority to the (low) beam divergence and diffraction experiments are mainly interested in intensity(ph/s/mm<sup>2</sup>). In practice one has to calculate the brilliance of the focus considering the properties of the insertion device(undulator, wiggler), the thermal deformation of optical elements, aberrations, polishing errors of mirrors and losses in windows and detectors. In the following we will consider the requirements for time-resolved diffraction and calculate the number of photons which can be delivered to a sample in a single pulse.

The insertion device consists of an array of alternating magnets, which forces the electrons into a sinusoidal motion about the incident direction[4]. When the electron beam is send through a vertically oscillating field of wavelength  $\lambda_0$ ,

$$B_z = B_0 \sin\left(2\pi \frac{x}{\lambda_0}\right),$$

the tangent to the orbit(or angular deflection) is:

$$\beta_y(x) = -\frac{K}{\gamma} \cos\left(2\pi \frac{x}{\lambda_0}\right),$$

where  $\gamma$  is the relativistic parameter  $(1-\{v/c\}^2)^{-1/2}$ ,  $\gamma = 1957 E(\text{GeV})$ . The deflection parameter K is defined

as

$$K = \frac{e B_0 \lambda_0}{2\pi m c} = 0.934 B_0(T) \lambda_0(\text{cm}),$$

where  $e$  is the electron charge and  $m$  it's mass. Note that the tangents fall within a cone of opening angle  $\pm K/\gamma$  around the mean forward direction.

The amplification in an undulator is caused by constructive interference from single electrons. In the curved part of the orbit, the electron releases polychromatic radiation, which moves forward along the tangent at the speed of light. The electron, which moves nearly at the speed of light, follows the longer sinusoidal trajectory imposed by the magnetic field. Those frequencies in the spectrum, that oscillate in phase with the reappearance of the electron, interfere constructively. The uneven harmonics are the strongest and appear at the wavelengths

$$\lambda_n = \frac{1 + K^2/2 + (\gamma\theta)^2 + (\gamma\varphi)^2}{2n\gamma^2},$$

where  $\theta$  and  $\varphi$  are the off-axis angles in the horizontal and vertical directions respectively. Numerically,

$$\lambda_n(\text{A}) = 13.056 \lambda_0(\text{cm}) \frac{1 + K^2/2 + (\gamma\theta)^2 + (\gamma\varphi)^2}{n E^2(\text{GeV})},$$

with the corresponding energy

$$\varepsilon_n(\text{keV}) = 0.95 \frac{n E^2(\text{GeV})}{\lambda_0(\text{cm}) \{1 + K^2/2 + (\gamma\theta)^2 + (\gamma\varphi)^2\}}$$

The on-axis spectrum of a single electron is the sum of uneven harmonics. When the acceptance angle of the aperture is relaxed(finite values of  $\theta$  and  $\varphi$ ), the harmonics are shifted to lower energies. The result is a triangularly shaped energy band with an upper cut-off given by the on-axis energy. In reality the bandwidth is further broadened by the energy and angular dispersion of the electron beam. The spectrum of a 235-pole undulator with a 17 mm period and a K of 0.86 is shown in fig. 3. In the following we shall call this undulator U17.

The angular distribution of the nth harmonic is concentrated in a cone of RMS width:

$$\sigma_r = \frac{1}{\gamma} \sqrt{\frac{(1 + K^2/2)}{2Nn}},$$

where N is the number of periods. Note that the opening angle is proportional to  $1/\sqrt{N}$ . The value of  $\sigma_r$  at the fundamental of U17 is 6.5  $\mu\text{rad}$ . The final divergence of the photon beam is the convolution of  $\sigma_r$  and the electron divergence. At the ESRF, the electron beam is focused in the centre of the straight section, under the conservation of emittance, into so-called low  $\beta$  and high  $\beta$  spots(or sites). The beam parameters are shown in table 2. Note that the vertical values are identical between the two sites. With a vertical electron divergence of 3.9  $\mu\text{rad}$ , quadratic convolution gives a photon beam of 7.6  $\mu\text{rad}$  for both sites. In contrast, the horizontal electron divergence is 87.8  $\mu\text{rad}$  and 12.3  $\mu\text{rad}$  on the low- and high  $\beta$  site respectively. The large horizontal divergence on the low  $\beta$  site is due to strong horizontal focusing. In the case of the U17, the horizontal divergence of the photon beam is dominated by the electron beam. The advantage of the low  $\beta$  site is the small RMS source size of 56.5  $\mu\text{m}$ h and 10.2  $\mu\text{m}$ v. The beam is readily focused by a toroidal mirror into a spot with the size of a typical protein. On the high  $\beta$  site, on the other hand, the cone is close to the single electron value and the spectral flux is enhanced due to the lower red shift. However, the enhancement comes at the cost of a large and elongated source: 391.7  $\mu\text{m}$ h and 9.8  $\mu\text{m}$ v. The horizontal and vertical focusing is therefore usually done independently.

The spectral flux in the central cone of the nth harmonic produced by a filament electron beam is:

$$I_n(\text{ph} / \text{s} / 0.1\% \text{bw}) = 1.432 \times 10^{14} N I(A) Q_n(K)$$

Here  $I(A)$  is the current in Amperes and

$$Q_n(K) = (1 + K^2 / 2) F_n(K) / n$$

where

$$F_n(K) = \frac{n^2 K^2}{(1 + K^2 / 2)^2} \left\{ J_{(n-1)/2} \left( \frac{n K^2}{4(1 + K^2 / 2)} \right) - J_{(n+1)/2} \left( \frac{n K^2}{4(1 + K^2 / 2)} \right) \right\}^2.$$

$J_n(x)$  is a Bessel function of the first kind. These functions are shown in fig. 4 and 5. Note that  $I_n$  is linear in N but independent of E. It is seen from fig. 4 that when  $0 < K < 0.5$ , the spectrum is dominated by the first harmonic. The tunability of  $E_f$  is limited but in return, the heatload is low. For values of K above 0.5, higher harmonics start to appear due to the increasing hardness of the spectrum at the turning points ( $E_c = 0.665 E^2(\text{GeV}) B_0(\text{T})$ ). The tunability and heatload are increased.

For experiments that use the unfocused beam, the figure of merit is central brightness:

$$\frac{d^2 I_n(0, 0)}{d\theta d\phi} (\text{ph} / \text{s} / 0.1\% \text{bw} / \text{m}r^2) = 1.774 \times 10^{14} N^2 E^2(\text{GeV}) I(A) F_n,$$

which is linear in  $N^2$  and  $E^2$ . The  $E^2$  dependence comes from the  $1/\gamma$  angular scaling and  $N^2$  from the angular reduction of the central cone with the number of periods. Note that each harmonic has a maximum at a given K. The brightness of a single harmonic undulator is thus  $K = 1.20$ .

The magnetic field in the insertion device is normally provided by strong permanent magnets such as NdFeB and SmCo, which produce fields in the 2T range. In practice one needs as many periods per unit length of straight section as possible. However, as the period becomes shorter, adjacent poles start to cancel out. The effect is accounted for by the Halbach equation[5]:

$$B_0 = B_1 \exp\left(-\pi \frac{g}{\lambda_0}\right),$$

where  $B_1$  is the saturation field, the field at zero gap.  $B_1$  depends on the magnet material. The latest insertion devices, which work with magnets inside the vacuum vessel, use SmCo magnets with  $B_1 = 1.65$  T[6,7]. Recent tests have shown that the gap can be lowered to 4.5 mm without any measurable effect on the electron beam. In practice the minimum operation gap of these devices is 6.0 mm. We list the characteristics of some of the new in-vacuum undulators in table 3.

In designing a beamline for specific experiments one will often have to compromise the performance of the insertion device. In cases where one can live with a limited tunability, a single harmonic undulator is usually best due to its low divergence and heatload. Alternatively, the same energy may be extracted from the third harmonic of a longer period device. That is done at the cost of higher divergence and heatload. In table 3 it is seen that one can obtain the same flux at 30 keV from the fundamental of a 11.0 mm undulator as the third harmonic of a 20.1 mm undulator. The single electron divergence is the same in both cases, but the tunability of the 20.1 mm undulator is much higher. The heatload of 3.84 kW is however a challenge.

The figure of merit for single bunch diffraction experiments is the spectral flux in a 0.1% bandwidth. The ESRF undulators produce here up to  $4 \times 10^8$  ph/0.1%bw/pulse, see table 2. The corresponding value for the fundamental of an undulator based on self amplified stimulated emission(SASE) in a free electron laser(FEL) facility is  $1 \times 10^{13}$  ph/0.1%bw/pulse in 200 fs. In addition the FEL divergence is in ca 20  $\mu$ rad. The FEL source is highly monochromatic and therefore, at first sights, not suitable for Laue diffraction. However, the spectrum of a FEL undulator has a background from the spontaneous emission with an amplitude of  $1 \times 10^8$  ph/0.1%bw/pulse, comparable to an ESRF in-vacuum undulator.

**TABLE 3.** Radiation characteristics of ESRF undulator based on SmCo magnets. The flux on the first and third harmonic is calculated for a single bunch current of 16 mA. The magnets are placed in the ring vacuum and the gap is 6.0 mm. The spectral flux from the fundamental of these undulators represents the present flux limits at the ESRF.

$E_f$ (keV)	K	$\lambda_0$ (mm)	2N	P(kW/200 mA)	$I_1$ (ph/0.1%bw/pulse)	$I_3$ (ph/0.1%bw/pulse)
10.0	1.21	20.1	200	3.84	4.24E+08	1.04E+08
15.0	0.86	16.9	236	2.71	3.53E+08	3.84E+07
20.0	0.62	14.6	275	1.89	2.60E+08	1.06E+07
30.0	0.31	11.0	363	0.82	1.03E+08	3.53E+05

The insertion devices presently used on ID09 are listed in table 4 and their spectra shown in fig. 6. It shows the focused flux from the U20 undulator and W70 wiggler. The beams are focused by a platinum coated toroidal mirror which receives a 10 mmh x 1.4 mmv beam 30 m from the source. The incidence angle is 2.335 mrad and the energy cut-off 38 keV. The monochromatic flux from a silicon(111) monochromator is derived by applying the relative bandwidth  $1.4 \times 10^{-4}$ . The y-axis on the left shows the intensity from one 150 ps pulse produced by one 16-mA bunch. Note the low flux below 7 keV caused by the attenuation in the default windows in the beamline( 1.0 mm beryllium and 0.26 mm graphite).

**TABLE 4.** Insertion device parameters for ID09, ESRF. The fwhm size of the electron beam the low- $\beta$  site is 0.117 mmh and 0.024 mmv. The U17 in-vacuum undulator will replace the U20 and U46 in July 2001.

ID	gap (mm)	$E_f$ (keV)	$E_c$ (keV)	K	2N	P(W/200 mA)
U20	16.3	16.70	3.5	0.27	162	160
U46	16.0	0.64	15.6	2.76	71	3116
W70	20.1	0.32	20.0	5.43	43	4788
U17	6.0	14.84	13.2	0.86	235	2740

## 4. Optics for picosecond experiments

### 4.1 Introduction

The main aim of the optics in a beamline is to monochromatise and focus the beam onto the sample with a minimum loss of emittance. That is a challenging task since the first optical elements at the ESRF are placed 26 m from the source in order for the vacuum chambers to stay clear of the electron beam. The focus point is therefore always far from the source which imposes strict tolerances on the stability of the optics. In addition the heatload on the optics, which can reach several kilowatts, has to be removed efficiently in order to conserve the emittance. The use of silicon crystals at cryogenic temperatures, where the ratio of the thermal expansion to thermal conductivity is low (or even zero), has by and large solved the heatload problem for monochromators. It appears however that future in-vacuum undulators, which can produce power densities in excess of  $100 \text{ W/mm}^2$ , will push the liquid nitrogen technique to the limit.

The pulse structure of synchrotron light is determined by the bunch structure of the electron beam and one needs a microsecond shutter to isolate single pulses from the storage ring. The ID09 beamline has a set-up for pump and probe experiments in Laue diffraction from macromolecules, oscillation diffractometry from small molecules, diffuse scattering from liquids, surface melting of semiconductors and x-ray spectroscopy in dilute systems. The photo excitation is done by a phase-locked femtosecond laser which runs synchronously with the x-rays and the chopper at 900 Hz. The polychromatic option for Laue diffraction is particularly difficult due to the high heatload in the focused beam. A system of three shutters, the first of which is water-cooled, is needed to isolate single pulses. The layout of the optics is shown in fig. 7. In the polychromatic mode, the toroidal mirror is inserted at an incidence angle of 2.335 mrad and the beam is focused into a  $\varnothing 250 \mu\text{m}$  spot 56.5 m from the source. The bandwidth is 6-38 keV. The monochromatic beam is produced by a double-bounce Bragg-Bragg monochromator downstream the toroidal mirror. The orthogonal distance between the two crystals is kept fixed at  $\rho = 10 \text{ mm}$ . The monochromatic beam is off-set downwards by  $\rho \sin(2\theta)/\sin(\theta)$  and the height of the table carrying the shutters and the sample is adjusted accordingly. The focused beam is now sent through the shutter system that is placed ca 1.2 m from the focal point. In the following we will describe the mirrors, the monochromator and the shutter system.

### 4.2 The focusing mirrors

The white beam is focused by a cylindrical mirror, which can be bent vertically into a toroid (and therefore called the toroidal mirror). The mirror is placed 29.7 m from the centre of the straight section. The second mirror is a 1.2-m long plane mirror, which is bent vertically into a parabola. The latter is used for micro-focusing experiments (for example, high pressure experiments in geophysics that employ a diamond anvil cell), but it is also used occasionally for time-resolved experiments when large and homogeneous beams are required. Both mirrors are water-cooled with heat extraction from the sides. The cooling system for the cylindrical mirror includes a copper roof which is lowered into the cylindrical cut of the mirror. The roof absorbs the Compton scattering and provides a heat shield for the bending mechanism. The mirror parameters are summarized in table 1. The 1000-mm long toroidal mirror was the first mirror received at the ESRF in 1992 (and it will soon be replaced by a pure silicon mirror). The body of the mirror is made of graphite enclosed in a SiC jacket. The slope error in the middle of the mirror is  $4.1 \mu\text{rad(rms)}$  over a length of 380-mm, which is substantially better than the average of  $9.0 \mu\text{rad(rms)}$ . In practice the intensity of the focus does not receive any radiation from the two outer parts of the mirror, a problem that is aggravated by strain from the mirror holder. The reflected powers were measured using a calorimeter and found to be 50 and 60% of the expected value for the toroid and parabolic mirror. That indicates that the surfaces are degraded due to micro-cracks and the deposition of impurities from the vacuum. The vacuum vessel for the toroidal mirror is pumped by two ion pumps and the pressure has now, after five years of pumping reached  $1 \times 10^7$  torr. By contrast the vacuum properties of the second mirror are much better due to the high purity of single-crystal silicon. The pressure is here  $2 \times 10^8$  torr.

**TABLE 5.** Mirror parameters

item	mirror 1	mirror 2
shape	cylindrical(toroidal)	plane(parabolic)
dimensions : L x W x H(mm <sup>3</sup> )	1000 x 130 x 100	1200 x 100 x 50
material	SiC on a graphite body	Si(single-crystal)
sagittal radius(mm)	64.53	-
coating	Pt	Pt
surface roughness(A; rms)	1.8	1.0
incidence angles (mrad)	2.335	1.25-5.0
energy range(keV)	5-38	5-55
source-mirror distance(m)	28.1; 29.7; 31.3	33.9; 35.5; 37.1
mirror-focus distance(m)	26.8	7.0
demagnification M	0.85-0.95	0.2
slope-error( $\mu$ rad; rms)	9.0(4.1 over 380 mm in the center)	6.0
gravity sag(km)	4.7	6.9
bending range(km)	1.8-4.7	1.5-6.9
pushing range(km)	4.7- $\infty$	6.9- $\infty$

The cooling of the mirrors works very well for the single-harmonic undulator U20 where the focal spot can be stable to within  $\pm 20 \mu\text{m}$  for several days. This is partly due to the low power of the U20 but also due to the good matching between the polychromatic spectrum and the mirror cut-off. In fact the stability of the focal spot is directly related to the heatload and the wiggler, with its greater power and content of hard radiation, turned out to be difficult to stabilise. However given that the exposure times in polychromatic experiments are very short, we decided to install a shutter in front of the toroidal mirror which can deliver shots down to 20-ms, see also fig. 7. It consists of a tunnel in a block of copper. It is driven by a stepper motor and the cooling water runs through the rotation axis. It can generate shots at frequencies up to 1 Hz. This shutter has completely solved the drift problem, which has given us more beamtime for experiments.

### 4.3 The Monochromator

The beamline has a water-cooled monochromator, which is designed to operate between 4.9-39.6 keV. The water cooling can extract up to 75 Watt before the rocking curve begins to broaden. It is mainly used with the U20 undulator and occasionally with the U46 and W70 at reduced currents(single bunch mode). The thermal slope-error of the first crystal was studied in order to increase the throughput of the monochromator. It was found that the best crystal geometry is a U-shaped cross-section with the footprint at the bottom of the U and cooling contacts at the top. That reduces thermal gradients in the longitudinal direction.

The distance between the diffracting surfaces is fixed ( $\rho = 10.0 \text{ mm}$ ) which makes the vertical position of the monochromatic beam a function of the Bragg angle ( $\delta h = -\rho \sin 2\theta / \sin \theta$ , with  $\rho = 10.0 \text{ mm}$ ). The height of the experimental table is adjusted accordingly and energy scans can be effectuated linking the Bragg angle to the table height. The two crystals are mounted in a mechanical frame with a weak mechanical link, which allows adjusting the angle of the second crystal. That frame is mounted onto a rotation table which is driven from outside the vacuum. The horizontal beam position is controlled at two levels: a stepper motor tilts the first crystal and a piezo tilts the second with high resolution.

The rejection of harmonics has to be considered due to the fixed energy cut-off at 38 keV of the toroidal mirror. In the range 4.5-12.7 keV, the (333) reflection contaminates the beam. The problem can be solved by opening the gap of the undulator hereby reducing the content of hard radiation.

The U17 undulator foreseen for ID09 in 2001, will produce a total power up to 2740 W and a power density up to  $110 \text{ W W/mm}^2$ . Final element analyses has shown that at these power densities, the deviation from crystal planarity becomes close to the rocking width of Si(111) even at cryogenic temperatures( $15 \mu\text{rad}$  at 15 keV). The monochromatic fluxes are summarised in table 6.

**TABLE 6.** The flux of the monochromatic beam from the U20 undulator ( $E_i = 16.45$  keV) using the ESRF single bunch mode at 16 mA.

item	
Tunability range(keV)	4.9-39.6
Resolution(eV)	4.3
Focal size(mmh x mmv)	0.18 x 0.20
Flux(ph/s @ 200 mA)	$1.8 \times 10^{13}$
Flux(ph/pulse)	$4.1 \times 10^5$
Stroboscopic flux(ph/s @ 896.6 Hz)	$3.6 \times 10^9$

#### 4.4 The Chopper System and its Synchronisation

The chopper was originally built for single bunch selection from the single bunch mode and hybrid mode at the ESRF. The main challenge was the extremely short time between pulses from the synchrotron. For example, in the multi bunch mode, x-rays arrive every 2.84 ns, impossible to isolate mechanically. The only usable modes at present are the 1-bunch, the 16-bunch mode and the hybrid mode. The time between pulses is 2.816  $\mu$ s, 0.176  $\mu$ s and 0.470  $\mu$ s respectively. The chopper consists of a triangular titanium disk with a channel carved along one of the sides. A three dimensional picture is shown in fig. 8 and the chopper performance is summarised in table 6. The triangular geometry is a compromise between high tip-speed and low inertia. The chopper rotates in vacuum at 896.6 Hz and the disk is held by magnetic bearings. The rotation frequency is the 396<sup>th</sup> sub harmonic of the orbit frequency. It is controlled by an active feed back system which can stability the rotor down to a  $\delta\omega/\omega$  of  $1 \times 10^{-5}$ . The speed at the tips is 545.3 m/s, thus exceeding the speed of sound in air. Consequently the devise has to be kept in vacuum. The shaft of the chopper exhibits a resonance at 998 Hz and the breakdown frequency of the disk is predicted to be 1300 Hz. It is thus impossible with this design to obtain shorter opening times by increasing the frequency.

The acceptance profile of the rotating chopper is trapezoidal. The base line  $\tau$  and opening profile  $p(t)$  are:

$$\tau = \frac{a}{2 \pi R f \sqrt{1 - (h/R)^2}}$$

and

$$p(t) = \begin{cases} 0 & \text{if } Abs[\theta(t)] \geq \theta_{min} \\ Min\left[1, \frac{2R}{S} \sin(\theta_{min} - \theta(t))\right] & \text{if } Abs[\theta(t)] \leq \theta_{min} \end{cases}$$

with

$$\theta_{min} = Arc \sin(a/2R) \quad \text{and} \quad \theta(t) = 2 \pi f t ,$$

where  $a$  is the tunnel height,  $R$  the maximum radius,  $h$  the perpendicular tunnel distance to the centre,  $f$  the rotation frequency and  $S$  the beam size. The base-line opening time can be calculated using the following parameters:  $a = 0.7$  mm,  $R = 96.8$  mm,  $h = 47.35$  mm,  $f_{max} = 896.64$  Hz which gives  $t_{min} = 1.472$   $\mu$ s. The first triangular rotor, which was made for the single bunch and hybrid mode, had a 0.7-mm high tunnel. However, in order to get more beamtime for picosecond experiments, we have now a new rotor with a trapezoidal cross section. Specifically, the new tunnel is 4.0 mm wide and its height increases linearly from 0.05 to 0.90 mm. The opening time can now be varied from 0.10 to 1.89  $\mu$ s by translating the chopper laterally which makes it possible to extract single pulses for the 16-bunch mode.

The rotor chamber is a 40 mm thick stainless steel cylinder which protects against rotor fracture. The cylindrical chamber is held in a frame, which allows the rotor & chamber to rotate in case of transient transfer of energy from the rotor. The chopper is mounted in a position & tilt alignment stage, which permits centring the chopper

very precisely on the x-ray beam. When a user stops the chopper, the controller automatically drives the rotor into the open position. A PC controls the chopper and it can be started from the lock-open position with one command. The rms phase jitter is displayed every two minutes and is typically 10.5 ns (rms) at full speed. The timing control of the chopper is based on an RF/8 (44MHz) signal, which limits the accuracy to 22 ns. The phase of the RF/4 signal can be scanned with 2.84 ns resolution from the general beamline control software SPEC. The chopper data are summarised in table 7.

**TABLE 7.** Chopper parameters

item	
Tunnel length(mm)	165.0
Maximum radius(mm)	96.8
Tunnel off-set(mm)	47.35
Minimum rotation frequency(Hz)	10.0
Maximum rotation frequency(Hz)	896.6
Tunnel width(mm)	4.0
Tunnel height(mm)	0.05 to 0.90
Minimum opening time: $\delta t_{\min}$ (sec)	$0.10 \times 10^{-6}$
Maximum opening time: $\delta t_{\max}$ (sec)	$0.17 \times 10^{-3}$
Phase jitter(sec)	$10 \times 10^{-9}$
Axial resonance frequency(Hz)	998
Centrifugal breakdown frequency(Hz)	1300

Note that the chopper selects single bunches at 896.6 Hz which corresponds to a pulse on the sample every 1.11 ms. In Laue experiments, the accumulation frequency is limited by the sample cooling and the Laue patterns are typically collected at a frequency of 1 Hz. We have therefore built a ms-shutter in front of the chopper. It consists of a 60 mm long bar with a trapezoidal tunnel along its length. The tunnel is 5 mm wide and the height increases linearly from 0.3 to 2.0 mm. The tunnel is centred on the axis of rotation, which gives two openings per turn. The bar is mounted on the axis of a stepper motor, which is mounted outside the vacuum via a ferrofluid feed-through. Normally this shutter is used in single-shot mode. Before the exposure, the tunnel is oriented downwards at  $-90$  degrees. The shortest exposure times are obtained by accelerating the tunnel from  $-90$  to  $+90$  degree and opening times down to 0.2 ms have been obtained.

The experimental front-end is shown in fig. 9. In the direction of the x-ray beam, it consists of a wire monitor (XBPM), a ms-shutter and a chopper, sample slits, an  $I_0$  monitor, a beryllium window, a transport pipe, a sample goniostat, a beamstop and a detector stage. Since some experiments require a quasi collinear excitation with the laser beam close to the x-ray beam, we displaced the sample slits 300 mm from the sample in order to have space for laser mirrors and lenses.

The synchronization principle for a Laue experiments is shown in fig. 10.

#### 4.5 The Femtosecond Laser System

The ID09 beamline has a femtosecond laser which is synchronised to the x-ray pulses to a jitter of 3-5 ps(RMS). It is being used for single bunch Laue diffraction, stroboscopic monochromatic data collection and finally to trigger a femtosecond streak camera(jitter free streak camera). The femtosecond laser system consists of three stages, see fig. 11. The first stage is a mode-locked Ti:Sapphire laser producing weak 100 fs pulses of 800 nm at a repetition of 88 MHz (RF/4). The mode-locking of the Ti:Sapphire oscillator is caused by an increase of the refractive index of as function of the intensity, also called the optical Kerr effect. For the high peak powers, the Ti:Sapphire crystal acts like a weak focusing lens. So the mode-locked beam has a narrower beam waist than the continuous beam.

In the next step the mode-locked Ti:Sapphire beam is used to seed a Ti:Sapphire chirped pulse amplifier (CPA), which generates after compression - 100 fs pulses of about 0.5 mJ per pulse at 900 Hz. It is called a

regenerative amplifier because the amplification compensates the lower repetition rate so that the input and output power is roughly the same.

Before the amplification step, the laser beam is in time stretched to 160 ps. The stretching of the pulse before amplification is necessary because the high electric field of a 100 fs pulse would lead to non-linear effects like self-focusing in the Ti:Sapphire crystal and in the pockels cell of the amplifier as its power builds up. Also, it would eventually exceed the damage threshold of the material. Once the pulse has left the amplifier and recompressed to 100 fs, self-focusing is no longer a problem since the optical components from then onwards work in transmission mode (beam splitters, lenses and non-linear crystals). However, in the amplifier it is necessary to send the pulse from 8 to 12 times through the 20 mm thick Ti:Sapphire crystal. The third stage is a frequency doubler, an optical parametric generator / amplifier (OPA), which can generate 460-760 nm light up to 35  $\mu\text{J}$  per pulse, and a third harmonic generator. The whole system is laid out on a 4.25 x 1.5 m<sup>2</sup> optical table.

From table 8 it is seen that a laser pulse contains more than  $3 \times 10^{13}$  photons thus matching the number of CO binding sites in a 100 x 100 x 100  $\mu\text{m}^3$  myoglobin crystal. That makes it possible, at least in principle, to produce a reasonable degree of excitation. In practice we would like to have 5-10 times more photons to compensate for losses (absorption, reflectivity, quarter waveplates, capillary reflections etc.).

**TABLE 8.** The performance of the Ti:Sapphire laser. The pulse length is ca 150 fs.

	wavelength(nm)	energy(eV)	energy( $\mu\text{J}$ /pulse)	ph/pulse	ph/sec
1 harm.	800	1.55	750	3.0E+15	2.7E+18
2 harm.	400	3.10	150	3.0E+14	2.7E+17
3 harm.	267	4.64	25	3.4E+13	3.0E+16
OPG/OPA	420	2.95	35	7.4E+13	6.6E+16
OPG/OPA	760	1.63	35	1.3E+14	1.2E+17

## 5. Future experiments with a Free Electron Laser(FEL)

The use of single bunch techniques on synchrotrons has made it possible to conduct a large number of pump and probe experiments in physics, chemistry and biology with a time resolution down to 50 ps. Moreover, by the use of time resolved detectors such as a jitter free streak camera, it has been possible to study perturbations and phase transitions on the surface of semiconductors with 1-10 ps resolution. The most striking examples of the use of pulsed synchrotron radiation are the Laue studies on smaller macromolecules (MbCO[8], HbCO and PYP[9]). In these systems one can track the changes in the three dimensional structure near bindings sites and chromophores with 100 picosecond resolution. The main difficulty has been that proteins are quasi opaque at optical wavelengths, which makes it difficult to excite them. In practice most systems have been excited to within 10-20 %. Note that a displaced carbon molecule ( $Z=6$ ), excited to 15% will be diffract less than a hydrogen atom in the ground state. At low excitation levels, one is forced to accumulate many pulses of x-rays to improve the signal to noise. The signal to noise of a difference amplitude (excited minus non-excited state), is proportional to  $N_{\text{ex}} \times N^{1/2}$ , where  $N_{\text{ex}}$  is the number of excited molecules and  $N$  the number of incident x-rays.

The number of incident laser photons should be determined by the condition of having one photon absorbed per active site. In practice 100% excitation may be hard to achieve with an ultra short pulses (which will be of interest for an XFEL). When a highly intense 10 fs pulse enters a sample, some molecules are likely to be hit twice. The Einstein principle of stimulated emission tells us that double hit molecules are sent back to the ground state. It appears therefore that a sample saturated by an ultra short pulse, can not be excited beyond 50%. The situation is different for picosecond and nanosecond pulses where the molecules have time to change their spectrum during the pulse. For example, if the sample is bleached by the front of the pulse, the front molecules become invisible for those photons arriving later. To the extend that one can chose the

excitation wavelength, the absorption for a given sample should not exceed 10% in order to ensure a low longitudinal gradient.

Recently small organic crystals undergoing ultra-fast, light triggered phase transitions were excited with fs laser pulses at a frequency of 900 Hz and large relative changes in the diffraction amplitudes were observed. It would be very interesting to see if this approach can be extended to proteins? For such proteins, the Laue techniques could be replaced by monochromatic oscillation diffractometry with a significant gain in spatial resolution. It seems important to study the efficiency of near-infrared excitation including the use of two-photon absorption.

From table 9 it is seen that an XFEL undulator gives  $1 \times 10^{13}$  ph/0.1%bw/pulse in a 200 fs pulse as compared to  $3 \times 10^8$  ph/0.1%bw/pulse from a 200 ps synchrotron pulse. The XFEL delivers thus  $3 \times 10^4$  more photons per pulse than the ESRF. Note that the line width  $\delta E/E$  of the XFEL fundamental is  $1 \times 10^{-3}$  as compared with 1-15% of an ESRF undulator. An XFEL is spectrally pure and close to the  $1.4 \times 10^{-4}$  bandwidth of a silicon(111) crystal. However, the XFEL peak is sitting on a very broad polychromatic background at  $1 \times 10^8$  ph/0.1%bw/pulse, close to ESRF peak levels! One is likely therefore to maintain conventional monochromators on an XFEL.

**TABLE 9.** Comparison between the U17 undulator(low beta) and the expected performance of a free electron laser(XFEL) based on a 250 GeV linac at Desy.

-	ESRF	XFEL
fwhm bunch length(s)	$150 \times 10^{-12}$	$200 \times 10^{-15}$
spectral flux(ph/pulse/ 0.1%bw)	$3 \times 10^8$	$1 \times 10^{13}$
peak flux (ph/sec/0.1%bw)	$2 \times 10^{18}$	$1 \times 10^{26}$
average flux (ph/sec/0.1%bw)	$1.5 \times 10^{15}$	$2 \times 10^{18}$
Undulator band width(%)	1-15%	0.1%

The bunch structure of the XFEL at Desy consists of a 1.0 ms pulse containing 12000 mini pulses each separated by 80 ns. The next train arrives 200 ms later. In the following we will indicate how present synchrotron methods can be implemented on the XFEL at Desy.

**Laue diffraction:** An XFEL is not meant for Laue diffraction due to its monochromaticity. However, the SASE amplification can be quenched by a taper in the undulator gap and the background, which will correspond to a classical tapered undulator, can be used for Laue diffraction(high energies should be removed by a mirror). The unique feature of Laue diffraction is that the intensity is fully recorded by the polychromatic beam. A much better alternative is to induce a vertical dispersion of the monochromatic beam using a beryllium lens. Matching the vertical divergence to the crystal mosaicity will give the full intensity from a stationary crystal from the fully coherent beam. The signal to noise and resolution should improve substantially. The 5 Hz repetition rate is adequate for this technique since the protein crystal needs to cool down between laser shots. In general it would be nice to have an accumulating 2D-detector which could pick-up say the first 100 frames in the pulse train. As an example, the first frame could be a 200 fs time point, the second a 80 ns, the third a 160 ns etc. That would save time and reduce the radiation damage from the laser.

**Small molecule diffraction:** The experience from ESRF has shown that some electron transfer crystals that can run at frequencies up to 1000 Hz. That makes optimal use of our chopper and femtosecond laser and makes conventional monochromatic data collection with a 2D detector possible. We are expecting that this technique will give us 100 ps stills of the electron density at atomic resolution(1.2 Å). The 5 Hz repetition of the XFEL is non optimal. Nevertheless the global data collection time will be shorter by a factor of ca 150 as compared to the ESRF.

**Gas Phase Reaction[10]:** The fastest reactions are found in gas molecules free of friction from the environment. The association of molecules is usually studied using cold molecular beams where the reactants are brought together by weak Van de Waals forces. Intermediate states and the reaction product will show up on an area detectors as rings of diffuse scattering. The radial distribution function holds information about the chemical composition, bond lengths and their time dependence. In dissociation reactions all bonds are stretched synchronously and interesting effects such as the transition from ionic and covalent bonding may be observed. In general the interpretation of these experiments needs input from a model and theory. Gas phase reactions take place at low densities (pressures) and one would have liked to accumulate at 1000 Hz!

**Liquids:** The formation of a cage around photo-active molecules determines the rate constants of a reaction. The cage may trap and moderate the reaction products and hence promote recombination, which sometimes passes through hot molecular states. It would be of great value to measure the pair correlation function and determine the geometry and composition of the cage. In irreversible reactions, the liquid is delivered through a laminar jet at a speed such the sample is exchanged between shots. Here again 5 Hz accumulation is non optimal.

**Surface melting:** When the surface of a semiconductor is hit by an ultra short laser pulse, its reflectivity changes from that of a solid to a liquid. That has been interpreted as evidence for ultra fast surface melting. By combining surface and bulk diffraction, it should be possible to check the structural transition following non thermal melting induced by valence band electrons. The scientific case for surface melting is discussed in these proceedings by J. Larsson et al. The diffraction process may be recorded by a gated detector (avalanche diodes with a boxcar integrator). In this case one may use two x-ray pulses 80 ns apart. The first measures the non-excited state and the second the excited state. Collecting the two states quasi simultaneously should reduce the  $1/\omega$  shot-noise.

**X-ray spectroscopy:** On the shortest times scales, the structural rearrangements are fairly localised and a local probe such as EXAFS is a powerful probe especially in disordered systems of low complexity. The energy scan may be accomplished by a scan of the undulator gap or by changing the electron energy of the bunches, which is a fascinating new feature of an XFEL. The normalisation of these experiments is sensitive to the stability of the x-rays, the laser, the sample and the detector.

The time resolution in future pump and probe experiments on an XFEL undulator, is determined by the convolution of the x-ray and laser pulse length and their relative jitter. Note that the timing jitter between the laser and the x-rays at the ESRF is 3-5 ps (RMS). A femtosecond laser on an XFEL beamline will have to be seeded by the same laser that is used to create the electron bunches. And these pulses will have to be transported in vacuum to the beamline (in the x-ray pipe?).

The time resolved x-ray community is small but growing steadily. In order to strengthen the scientific case for a free electron laser, we encourage people to harvest the potential of existing picosecond facilities such as the ESRF, APS and SPring8.

#### References:

- [1] D. Bourgeois, T. Ursby, M. Wulff, C. Pradervand, A. Legrad, W. Schildkamp, S. Labouré, V. Srajer, T. Y. Teng, M. Roth and K. Moffat, *J. Synchrotron Rad.*, **3**, 65-74, 1996.
- [2] M. Wulff, F. Schotte, G. Naylor, D. Bourgeois, K. Moffat and G. Mourou, *Nuclear Instruments and Methods in Physics Research A* **398**, 69-84, 1997.
- [3] M. Wulff, P. Suortti, D. Häusermann, M. Hanfland

ESRF News Letter no **21**, 18-19 May, 1994.

- [4] The X-ray data booklet, Lawrence Berkeley Laboratory, Berkeley, PUB-490 Rev, 1986.
- [5] K. Halback, Nucl. Instrum. Methods, **187**, 109, 1981.
- [6] J. Chavanne, P. Van Vaerenbergh and P. Elleaume,  
Nuclear Instruments and Methods in Physics Research, **A 421**, 352-360, 1999.  
and  
J. Chavanne, P. Elleaume and P. Van Vaerenbergh, PAC99, **THA20**, 1999.
- [7] P. Elleaume and P. Berkvens(ESRF). Private communication.
- [8] V. Srajer, T. Teng, T. Ursby, C. Pradervand, Z. Ren, S. Adachi, W. Schildkamp, D. Bourgeois, M. Wulff and K. Moffat, Science, **274**, 1726-1729, 1996.
- [9] P. Perman, V. Srajer, Z. Ren, T. -Y. Teng, C. Pradervand, F. Schotte, D. Bourgeois, T. Ursby, M. Wulff, R. Kort, K. Hellingwerf and K. Moffat, Science, **279**, 1946-1950, 1998.
- [10] A. H. Zewail, Scientific American, 76-82, December 1990.

## Figure captions:

**Figure 1:** Filling modes at the ESRF. The availability, maximum current and lifetime is also shown. The lifetime is defined by the exponential decay  $I = I_0 \cdot e^{-t/\tau}$ .

**Figure 2:** The x-ray pulse length at ESRF measured by an optical Hamamatsu streak camera. With permission from Kees Scheidt, ESRF.

**Figure 3:** Spectrum of the focal spot from the in-vacuum undulator U17. The beam is focused by a platinum coated toroidal mirror 30 m from the insertion device. The acceptance aperture is 10 mmh and 1.4 mmv. The red curve shows the effect of a 1-mm taper, i.e. the gap is varied linearly from 6 mm at the entrance to 7 mm at the exit. The softer shape of the spectrum is important for the normalisation of Laue data. The polychromatic flux in one 16 mA pulse – integrated over the entire spectrum, is  $3.25 \times 10^{10}$  ph and  $2.53 \times 10^{10}$  ph with and without taper.

**Figure 4:** The flux in the central cone of a undulator is proportional to  $Q_n(K)$ . For values of K greater than 5, the device turn into a wiggler, i.e. a quasi continuous spectrum.

**Figure 5:** Central brightness of an undulator is proportional to  $F_n(K)$ . The curves give the amplitude distribution of the first, third, fifth, seventh and ninth harmonic.

**Figure 6:** The spectral flux of the focused of the insertion devices on ID09(Jan 2000).

**Figure 7.** Layout of optical components on ID09.

**Figure 8.** The Julich chopper used for single pulse selection.

**Figure 9.** The experimental front-end components.

**Figure 10.** The synchronisation of shutters in a Laue experiments

**Figure 11.** The femtosecond laser and the chopper and their phase locking to the RF clock

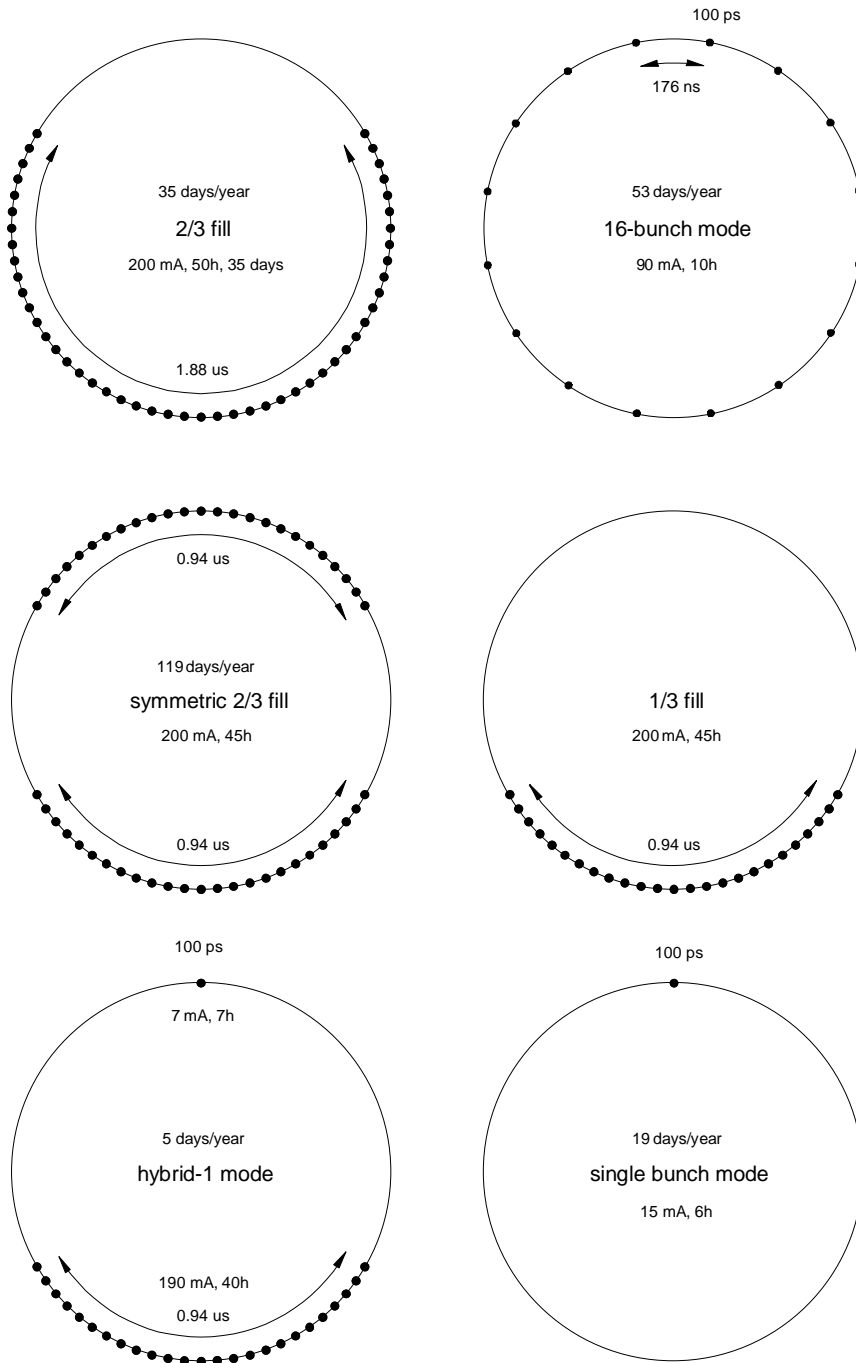


Figure 1

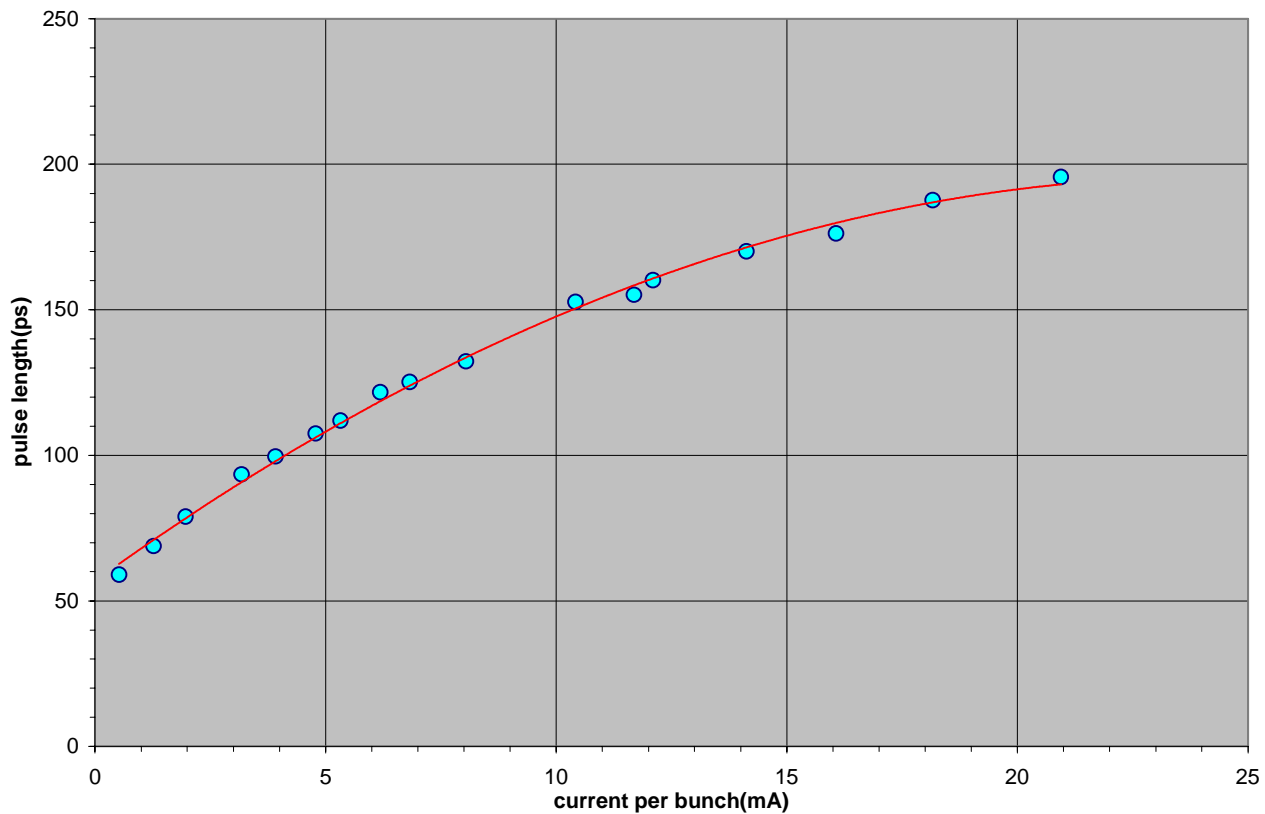


Figure 2

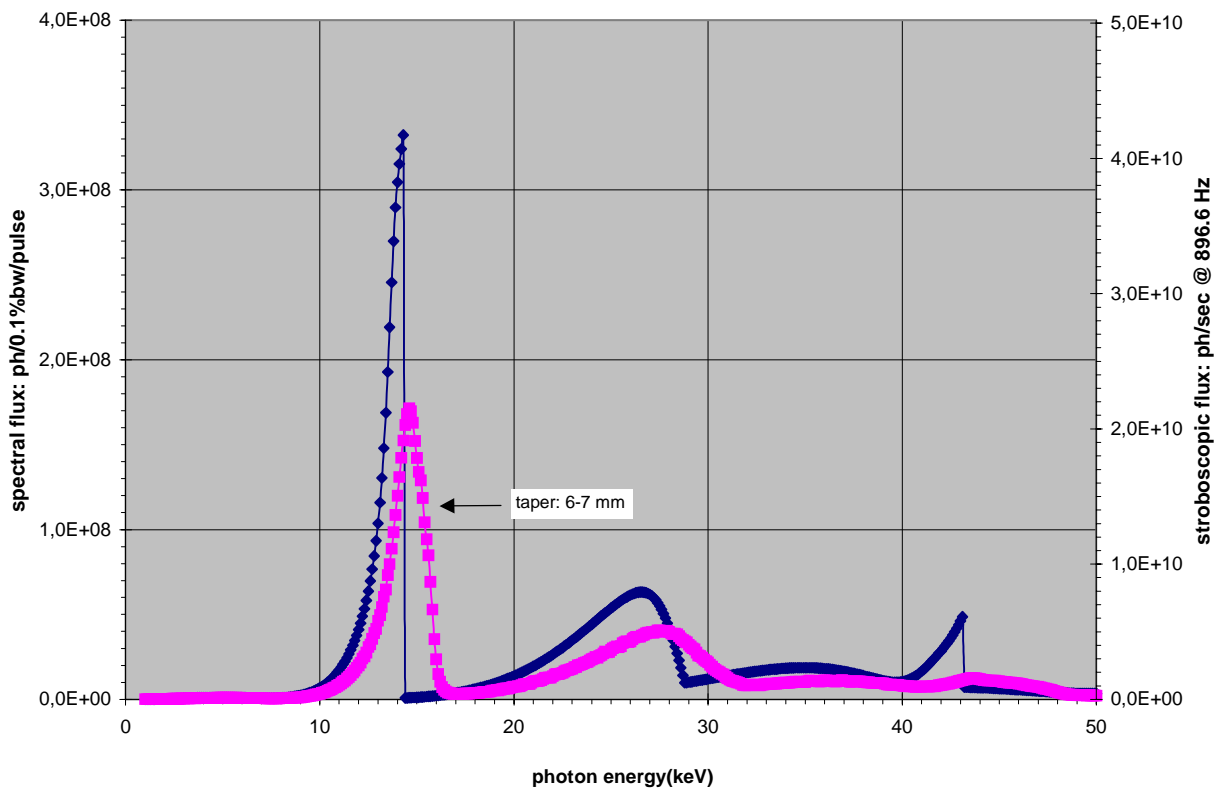


Figure 3

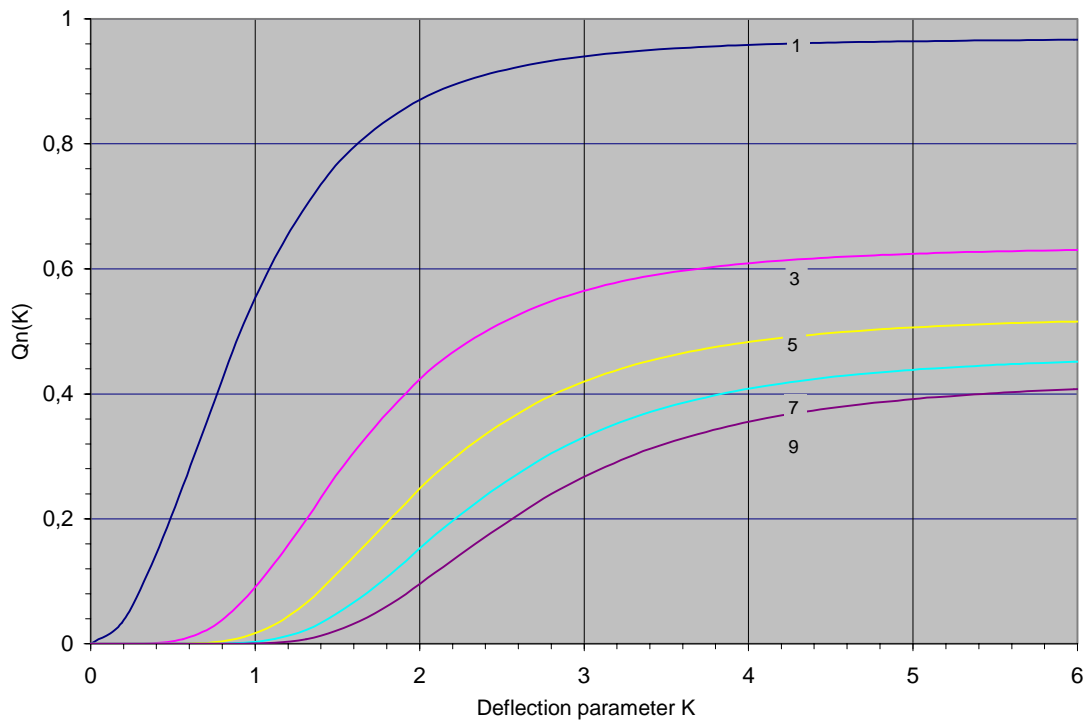


Figure 4

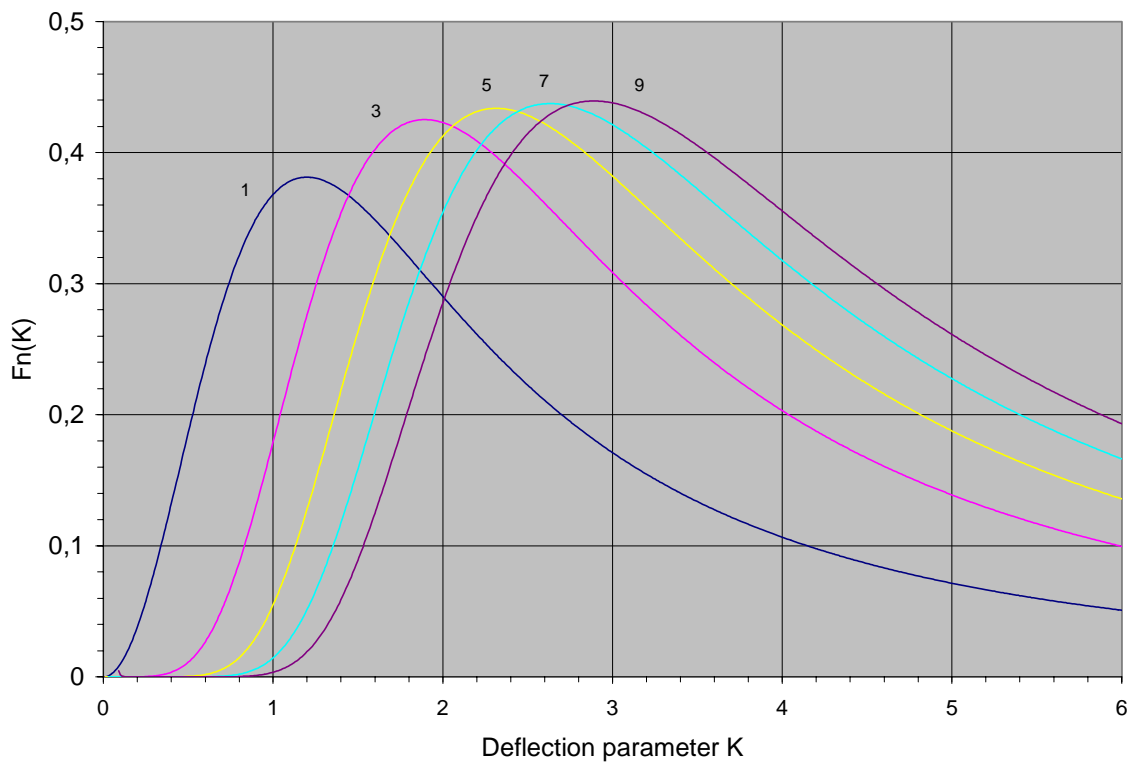


Figure 5

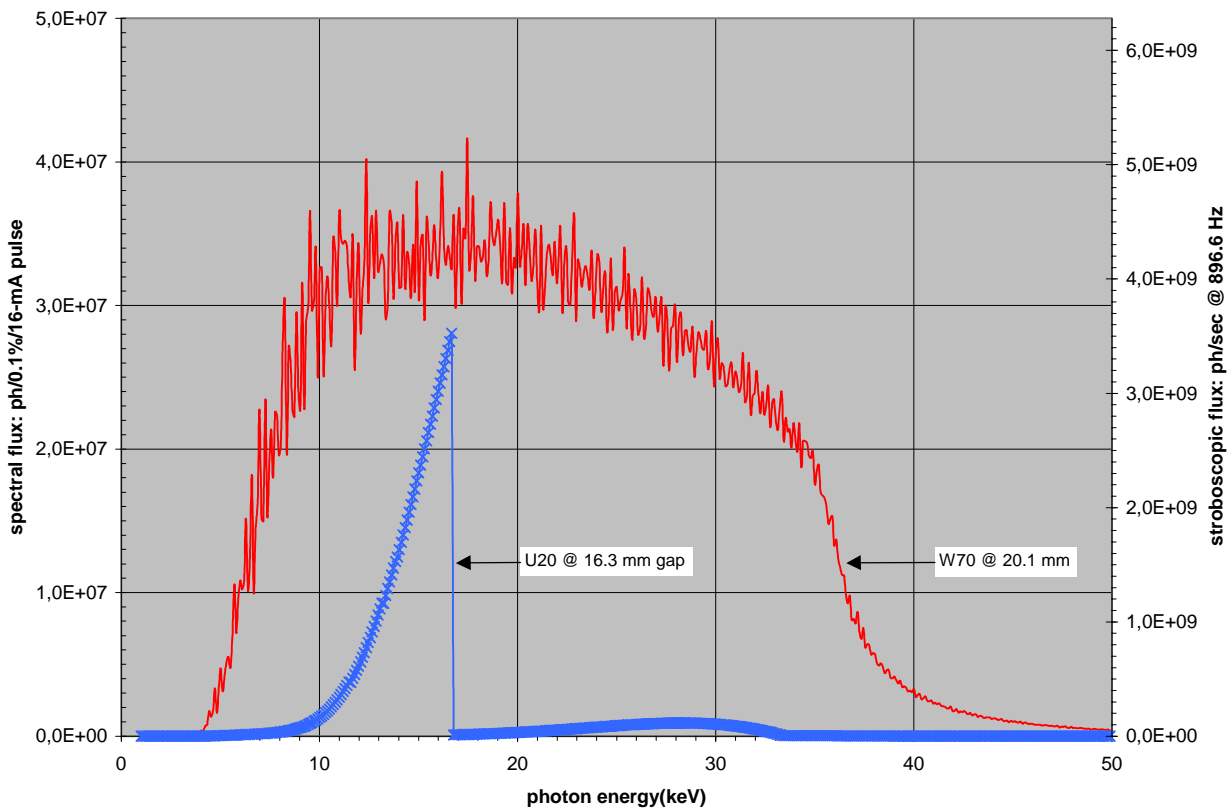


Figure 6

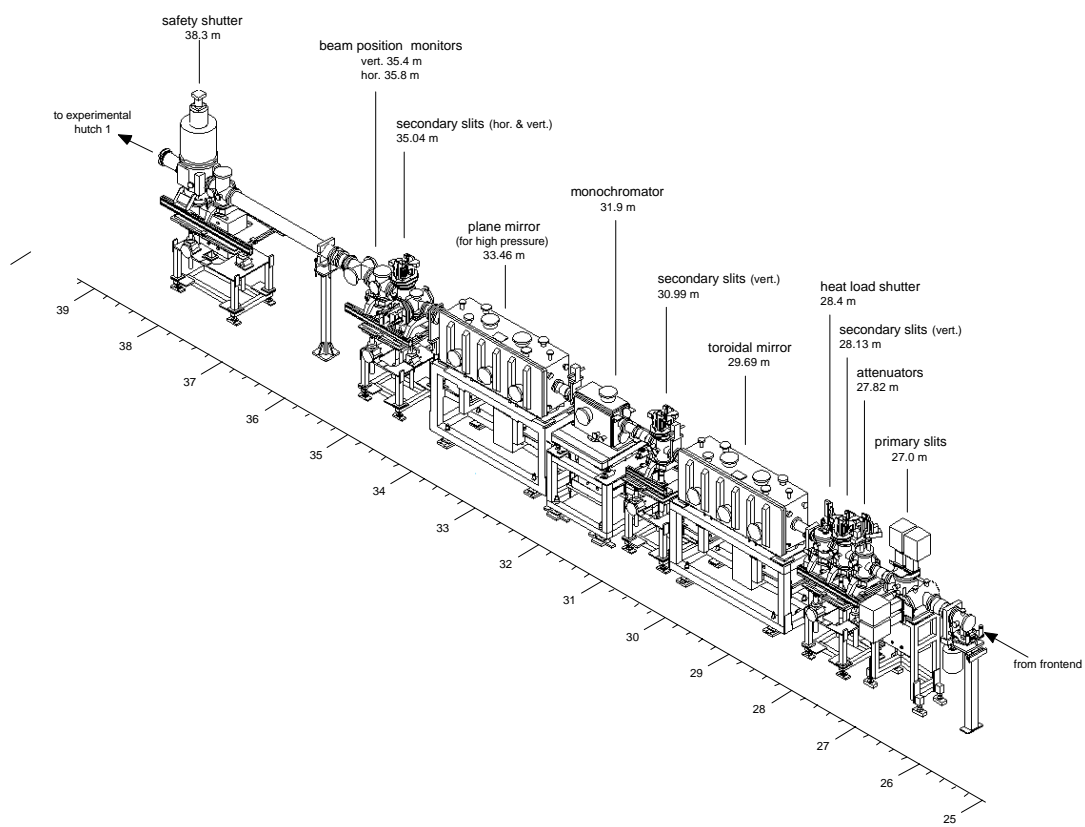


Figure 7

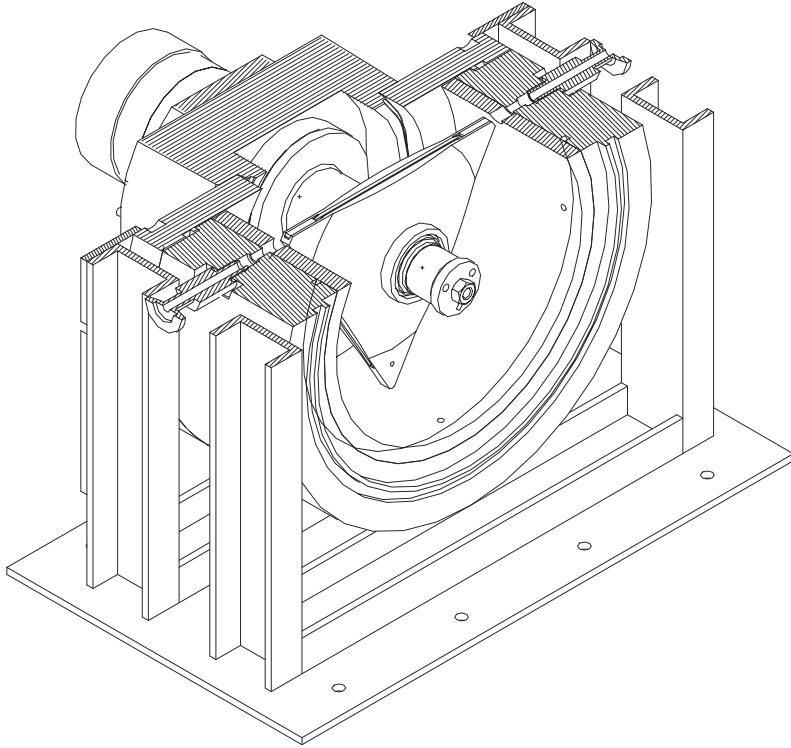


Figure 8

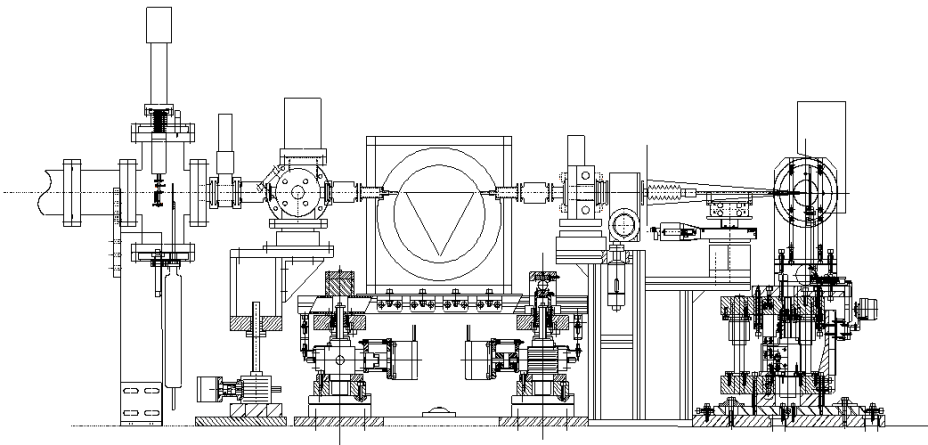


Figure 9

### Synchronisation of 4 shutters for 100 ps Laue diffraction

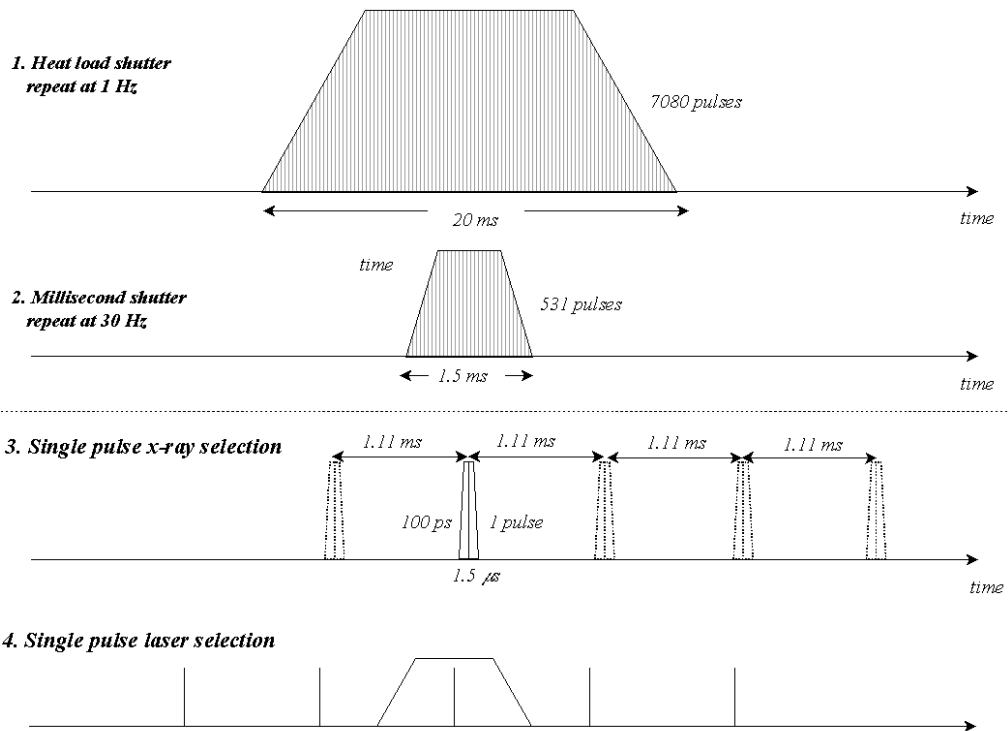


Figure 10

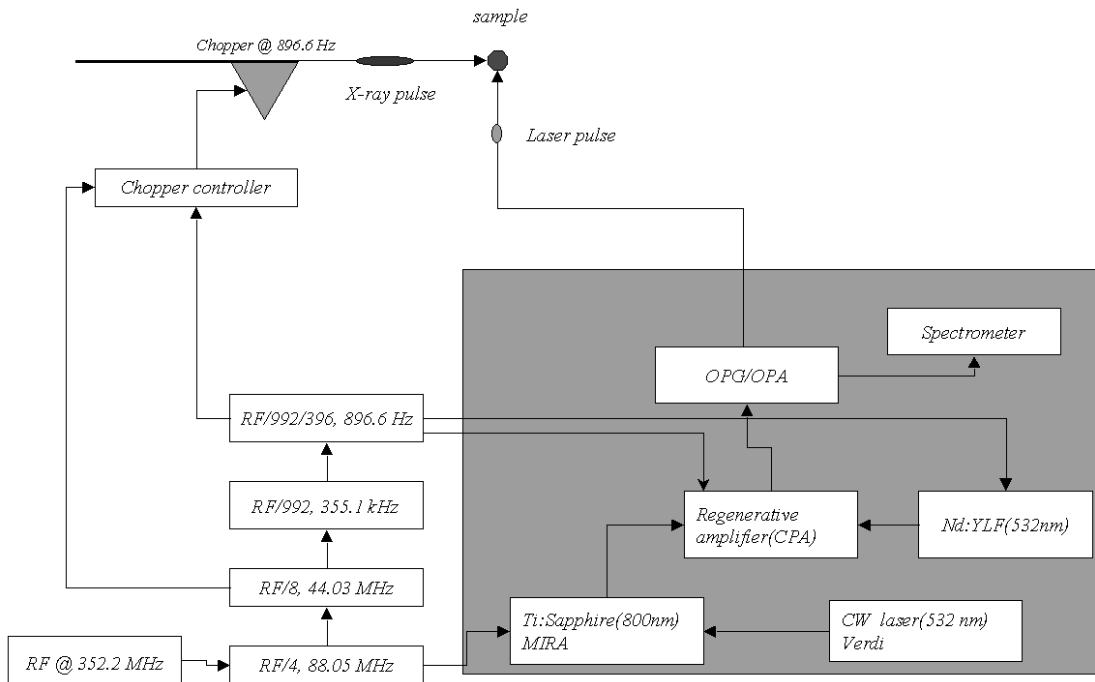


Figure 11